


Article

Platinum Palladium Bimetallic Nanozymes Stabilized with Vancomycin for the Sensitive Colorimetric Determination of L-cysteine

Han Zhao ^{1,2}, Kai Liu ¹, Lijie Zhou ¹, Tingting Zhang ¹, Zengsheng Han ^{1,*} , Longgang Wang ^{1,2,*}, Xianbing Ji ³, Yanshuai Cui ³, Jie Hu ¹ and Guanglong Ma ⁴

¹ Hebei Key Laboratory of Nano-Biotechnology, College of Environmental and Chemical Engineering, Yanshan University, Qinhuangdao 066004, China; han0325@stumail.ysu.edu.cn (H.Z.); d202210477@xs.ustb.edu.cn (K.L.); ljzhou@stumail.ysu.edu.cn (L.Z.); ttz@stumail.ysu.edu.cn (T.Z.); hujie@ysu.edu.cn (J.H.)

² State Key Laboratory of Metastable Materials Science and Technology, Yanshan University, Qinhuangdao 066004, China

³ Department of Environmental Engineering, Hebei University of Environmental Engineering, Qinhuangdao 066102, China; jixianbing@hebeue.edu.cn (X.J.); cuiyanshuai@hebeue.edu.cn (Y.C.)

⁴ Centre for Cancer Immunology, Faculty of Medicine, University of Southampton, Southampton SO16 6YD, UK; gm1c21@soton.ac.uk

* Correspondence: hanzs@ysu.edu.cn (Z.H.); lgwang@ysu.edu.cn (L.W.)

Abstract: Many diseases in the human body are related to the level of L-cysteine. Therefore, it is crucial to establish an efficient, simple and sensitive platform for L-cysteine detection. In this work, we synthesized platinum palladium bimetallic nanoparticles (Van-Pt_m/Pd_n NPs) using vancomycin hydrochloride (Van) as a stabilizer, which exhibited high oxidase-like catalytic activity. In addition, the catalytic kinetics of the Van-Pt₁/Pd₁ NPs followed the typical Michaelis–Menten equation, exhibiting a strong affinity for 3,3',5,5'-tetramethylbenzidine substrates. More importantly, we developed a simple and effective strategy for the sensitive colorimetric detection of L-cysteine using biocompatible Van-Pt₁/Pd₁ NPs. The detection limit was low, at 0.07 μM, which was lower than the values for many previously reported enzyme-like detection systems. The colorimetric method of the L-cysteine assay had good selectivity. The established method for the detection of L-cysteine showed promise for biomedical analysis.

Keywords: bimetallic; nanozymes; colorimetric; L-cysteine; detection



Citation: Zhao, H.; Liu, K.; Zhou, L.; Zhang, T.; Han, Z.; Wang, L.; Ji, X.; Cui, Y.; Hu, J.; Ma, G. Platinum Palladium Bimetallic Nanozymes Stabilized with Vancomycin for the Sensitive Colorimetric Determination of L-cysteine. *Biomolecules* **2023**, *13*, 1254. <https://doi.org/10.3390/biom13081254>

Academic Editor: Umesh Desai

Received: 11 July 2023

Revised: 5 August 2023

Accepted: 11 August 2023

Published: 16 August 2023



Copyright: © 2023 by the authors. Licensee MDPI, Basel, Switzerland. This article is an open access article distributed under the terms and conditions of the Creative Commons Attribution (CC BY) license (<https://creativecommons.org/licenses/by/4.0/>).

1. Introduction

L-cysteine is one of the sulfur-containing α-amino acids with good water solubility. Meanwhile, L-cysteine is involved in the reduction process of cells and phospholipid metabolism in the liver. The intracellular concentration of L-cysteine is usually around 30–200 μM [1]. High or low levels of L-cysteine in the body can cause diseases [2]. Therefore, it is important to establish an efficient, reliable and sensitive L-cysteine assay platform with which to detect its concentration. Currently, many methods have been reported for the detection of L-cysteine, including electrochemical methods, high-performance liquid chromatography, spin photometric methods, fluorescence detection and colorimetric detection [3–6]. However, many detection methods are limited in terms of their wide application by their cost, detection time, toxicity and environmental hazards.

In recent years, colorimetric detection has been considered as a promising method for the detection of L-cysteine due to its simplicity of operation and good visualization [7]. Many natural enzymes have been widely used in colorimetric assays. For example, Huang et al. [8] used the peroxidase activity of fig protease for the colorimetric assay

of L-cysteine. The application of natural enzymes was limited due to shortcomings such as their complex extraction process, fallibility and cost.

More recently, artificial enzymes with enzyme-like activities have been developed. Since the first study of Fe₃O₄ nanomaterials for peroxidase-like activity in 2007 [9], nanozyme-based colorimetric sensing platforms have contributed to the rapid development of the diagnostic and bioanalytical fields. A variety of nanozymes including noble metals [10], metal oxides [11,12], carbon-based materials [13,14] and other nanomaterials [15–18] have been reported. Pandey et al. [19] reported the structural characterization of noble metal monometallic, bimetallic and trimetallic nanoparticles, in addition to evaluating their biocatalytic activity for the non-enzymatic sensing of glucose. In particular, artificial nanozymes composed of noble metal nanoparticles have a wide range of applications due to their high interfacial stability, easy preparation and modification [20], as in the case of Pt nanotubes [21], gold nanoparticles [22] and Pd nanoparticles. Compared with monometallic nanoparticles, bimetallic nanoparticles with synergistic effects have received widespread attention because of their higher catalytic activity [23,24]. Jang et al. [25] reported a TiO₂-loaded Pt-Pd bimetallic model catalyst. Compared with the monometallic catalyst, the d electrons of Pt-Pd bimetallic nanoparticles were transferred from Pt 5d to Pd 4d upon alloying and the orbital hybridization and electronic state broadening of Pt and Pd. This led to a significant improvement in the catalytic performance of the bimetallic Pt-Pd catalyst. The metals Pt and Pd are both face-centered, cubic-structured metals with similar lattice constants; thus, they are more likely to form a homogeneous alloy. When Pt and Pd form an alloy, the coupling between the metals can improve their catalytic performance. Jin et al. [26] reported a Pd-Pt bimetallic alloy nanowire that exhibited excellent oxidase activity in an acidic environment.

Despite their small size, noble metal nanoparticles have a large specific surface area and high catalytic activity. But they tend to aggregate easily in solutions, leading to reduced activity. Therefore, the introduction of various carriers to stabilize small nanoparticles is considered one of the most effective ways to improve the catalytic activity and stability of enzyme mimics [27]. Among the nanoparticles, the carriers usually serve as a backbone to widely disperse and stabilize the active components, such as inorganic mesoporous silica [28], polymeric carriers [29] and polysaccharides, etc. [30]. Because of their good biocompatibility and easy modification, peptides have become a good means of modification on the surface of nanomaterials [31]. Vancomycin hydrochloride (Van), as an antibacterial peptide, is a glycopeptide antibiotic with a molecular weight of 1486 and has great potential for stabilizing precious metal nanoparticles.

In this study, we synthesized platinum palladium bimetallic nanoparticles (Van-Pt_m/Pd_n NPs, $m = 1, 2$; $n = 1, 2$) using Van as a biological template for the first time. The particle size of the Van-Pt_m/Pd_n NPs was around 5 nm. A high catalytic activity of the Van-Pt₁/Pd₁ NPs was achieved by exploring the preparation method and the molar ratio of platinum and palladium. Based on the Van-Pt₁/Pd₁ NPs' oxidase-like and peroxidase-like enzymatic activity, we developed a simple and effective colorimetric method for the determination of L-cysteine with a low detection limit, a wide detection range and good selectivity. Importantly, the use of Van may reduce the toxicity of noble metals, which may offer the possibility for the wide application of noble metal nanozymes.

2. Materials and Methods

2.1. Materials

Vancomycin hydrochloride (Van), potassium tetrachloroplatinate (K₂PtCl₄), sodium tetrachloropalladate (Na₂PdCl₄), sodium borohydride (NaBH₄), 3,3',5,5'-tetramethylbenzidine (TMB), H₂O₂, dopamine hydrochloride (DA·HCl), p-benzoquinone (BQ), sodium nitride (NaN₃), isopropyl alcohol (IPA), disodium ethylenediaminetetraacetate (EDTA-2Na) and dimethyl sulfoxide (DMSO) were purchased from Aladdin (Shanghai, China). The HeLa cell is a human cervical cancer cell line. Dialysis bags (MWCO = 14,000) were purchased from Laboratories Inc. (Piscataway, NJ, USA).

2.2. Synthesis of Van-Pt_m/Pd_n Nanoparticles

- (a) A total of 73 μL of Van solution (10 mM) was added to a 2 mL polyethylene (PE) tube, and then 98 μL of K_2PtCl_4 solution (10 mM) was added. The solution was incubated at 25 $^\circ\text{C}$ at 600 rpm for 12 h. Then, 10 μL of NaBH_4 solution (1 M, dissolved in 0.3 M NaOH solution) was added, and hydrochloric acid (1 M) was added to adjust the pH of the solution to approximately 7 after 3 h. Then, 48 μL of Na_2PdCl_4 solution (10 mM) was added, and 10 μL of NaBH_4 solution (1 M) was added after 12 h. After 24 h of dialysis, the product obtained was Van-Pt₂-Pd₁ NPs (Pt: Pd = 2:1).
- (b) The Van-Pd₁-Pt₂ NPs (Pt: Pd = 2:1) were prepared in a similar manner to the synthesis of Van-Pt₂-Pd₁ NPs. The order of the K_2PtCl_4 and Na_2PdCl_4 solutions was reversed.
- (c) One-pot method: Van (73 μL , 10 mM), K_2PtCl_4 (98 μL , 10 mM) and Na_2PdCl_4 (48 μL , 10 mM) solutions were mixed in PE tubes and kept at 25 $^\circ\text{C}$ for 12 h. Then, 20 μL of NaBH_4 solution (1 M, dissolved in 0.3 M NaOH solution) was added and kept at 25 $^\circ\text{C}$ for 12 h. The solution was dialyzed for 24 h to obtain Van-Pt₂/Pd₁ NPs (Pt: Pd = 2:1). We prepared Van-Pt₁/Pd₁ NPs in the same way (Pt: Pd = 1:1). The Pt₁/Pd₁ NPs were prepared in water, and the other conditions were the same as those for the Van-Pt₁/Pd₁ NPs.

2.3. Characterization of Van-Pt_m/Pd_n Nanoparticles

The absorbance in the wavelength range of 200–800 nm was measured with a UV-vis spectrophotometer. The morphology was photographed using transmission electron microscopy (TEM); the crystal structure of the nanoparticles was characterized using an X-ray diffraction (XRD) meter with a diffraction ratio of 10 $^\circ$ –90 $^\circ$; the elements and valence states of the nanoparticles were determined via X-ray photoelectron spectroscopy (XPS); and the hydrodynamic size and zeta potential were determined with a Zetasizer Nano-ZS90.

2.4. Activity of Van-Pt₁/Pd₁ Nanoparticles

The oxidase-like activity of the Van-Pt₁/Pd₁ nanoparticles was determined by measuring the oxidized TMB. A total of 200 μL of Van-Pt₁/Pd₁ nanoparticles ($C_{\text{Pt}} = 0.45$ mM) was added to a 2 mL PE tube. Then, 300 μL of 0.2 M HAc-NaAc solution (pH = 3) was added, and 1000 μL of 0.2 M HAc-NaAc solution containing 0.6 mM TMB was added. The samples were incubated in a constant-temperature mixer at 25 $^\circ\text{C}$ and 600 rpm for 5 min. The absorbance was measured using a UV-vis spectrophotometer. In addition, the relative activity of the Van-Pt₁/Pd₁ NPs was determined at different pHs (pH = 1–12) and temperatures (5–65 $^\circ\text{C}$). The samples added to the PE tubes were varied according to the experimental requirements.

The peroxidase-like activity of the Van-Pt₁/Pd₁ nanoparticles was determined by assaying the oxidized TMB produced under hydrogen peroxide conditions. 200 μL of Van-Pt₁/Pd₁ nanoparticles ($C_{\text{Pt}} = 0.45$ mM) were added to a 2 mL PE tube. Then, 300 μL , 0.2 M of HAc-NaAc solution (pH = 3) was added; 1000 μL of 0.2 M HAc-NaAc solution containing 0.6 mM TMB was added, 100 μL , 0.03 M H_2O_2 solution was added. The samples were incubated in a constant temperature mixer at 25 $^\circ\text{C}$ and 600 rpm for 2 min. The absorbance was measured by UV-vis spectrophotometer.

2.5. Catalytic Kinetics of Van-Pt₁/Pd₁ Nanoparticles

In total, 200 μL of Van-Pt₁/Pd₁ nanoparticles ($C_{\text{Pt}} = 0.45$ mM) was added to a 2 mL PE tube. Then, we added 0.2 M of HAc-NaAc solution (pH = 3) and 0.2 M HAc-NaAc solution containing 0.6 mM TMB. The absorbance was measured using a UV-vis spectrophotometer. The amount of buffer solution was 1200–300 μL at 100 μL intervals, and the amount of buffer solution containing TMB was 100–1000 μL at 100 μL intervals. The total amount of

liquid in the PE tube was 1500 μL . The affinity for the substrate and the maximum rate of the catalytic reaction during enzyme catalysis was studied using Formula (1) [32].

$$v = \frac{V_m[S]}{K_m + [S]} \quad (1)$$

Here, V_m is the maximum reaction rate; $[S]$ is the substrate concentration; and K_m is the Michaelis–Menten constant.

2.6. The Mechanism of Oxidase-Like Activity

The types of reactive oxygen species (ROS) produced during catalysis were studied by adding different ROS inhibitors to the solution. A total of 200 μL of Van-Pt₁/Pd₁ NPs ($C_{\text{Pt}} = 0.45 \text{ mM}$) was added to a 2 mL PE tube. Then, 1000 μL of 0.2 M HAc-NaAc solution containing 0.6 mM TMB was added, and 200 μL of different solutions of reactive oxygen inhibitor solutions (10 mM) was added. The samples were incubated in a constant-temperature mixer at 30 °C and 600 rpm for 5 min. The absorbance was measured using a UV-vis spectrophotometer. The ROS inhibitors were p-benzoquinone (BQ), sodium nitride (NaN_3), isopropyl alcohol (IPA) and disodium ethylenediaminetetraacetate (EDTA-2Na), respectively.

2.7. Detection of L-cysteine Using Van-Pt₁/Pd₁ Nanoparticles

A total of 50 μL of Van-Pt₁/Pd₁ nanozymes ($C_{\text{Pt}} = 0.45 \text{ mM}$) was added to a 2 mL PE tube, followed by 1000 μL of 0.2 M, pH = 3 HAc-NaAc solution containing 0.6 mM TMB, and then 200 μL of aqueous L-cysteine solution at different concentrations. Then, the tube was placed in a constant-temperature reaction at 30 °C and 600 rpm for 5 min. Finally, the UV-vis spectrum was measured. The standard curve of the assay was obtained using the difference in absorbance versus concentration. The real samples were replaced with different samples with different concentrations of L-cysteine containing the spiked amount, and the recoveries were calculated according to the spiked recovery Formula (2) [33].

$$\text{recovery rate}\% = \frac{A_i - A_0}{A_i^* - A_0} \times 100 \quad (2)$$

A_i^* is the theoretical absorbance, and A_i is the actual absorbance.

2.8. Biocompatibility Test

The biocompatibility of the nanozymes was determined using the MTT method. First, cells were added to 96-well plates and incubated in a cell incubator for 24 h. Then, samples ($C_{\text{samples}} = 12.5\text{--}200 \mu\text{g/mL}$) including Van and Van-Pt₁/Pd₁ NPs were added to the 96-well tissue culture plates and incubated for 24 h. After that, MTT (100 μL , 500 $\mu\text{g/mL}$) was added. After 4 h, the MTT solution was removed, and DMSO solution was added. Finally, the absorbance of the 96-well plates was measured using a microplate reader.

3. Results and Discussion

3.1. Characterization of Van-Pt_m/Pd_n Nanoparticles

As shown in Figure 1A, a UV-vis spectrometer was used to scan the Van-Pt_m/Pd_n nanoparticles within 250–700 nm. The characteristic bands of Pt²⁺ were at 392 nm and 329 nm, and Pd²⁺ had a distinct characteristic absorption band at 420 nm. The Van-Pt_m/Pd_n NPs had no obvious characteristic absorption bands of Pt²⁺ or Pd²⁺, which may be because Pt²⁺ and Pd²⁺ were reduced to Pt and Pd, respectively. The mere absence of Pt²⁺ and Pd²⁺ transitions in the UV-vis spectra suggested that Van-Pt_m/Pd_n nanoparticles may have formed. In addition, the color of the Van-Pt_m/Pd_n NPs was brown (Figure 1B), similar to the color of previously reported Pt/Pd NPs [34]. All these results indicated the successful synthesis of Van-Pt_m/Pd_n NPs.

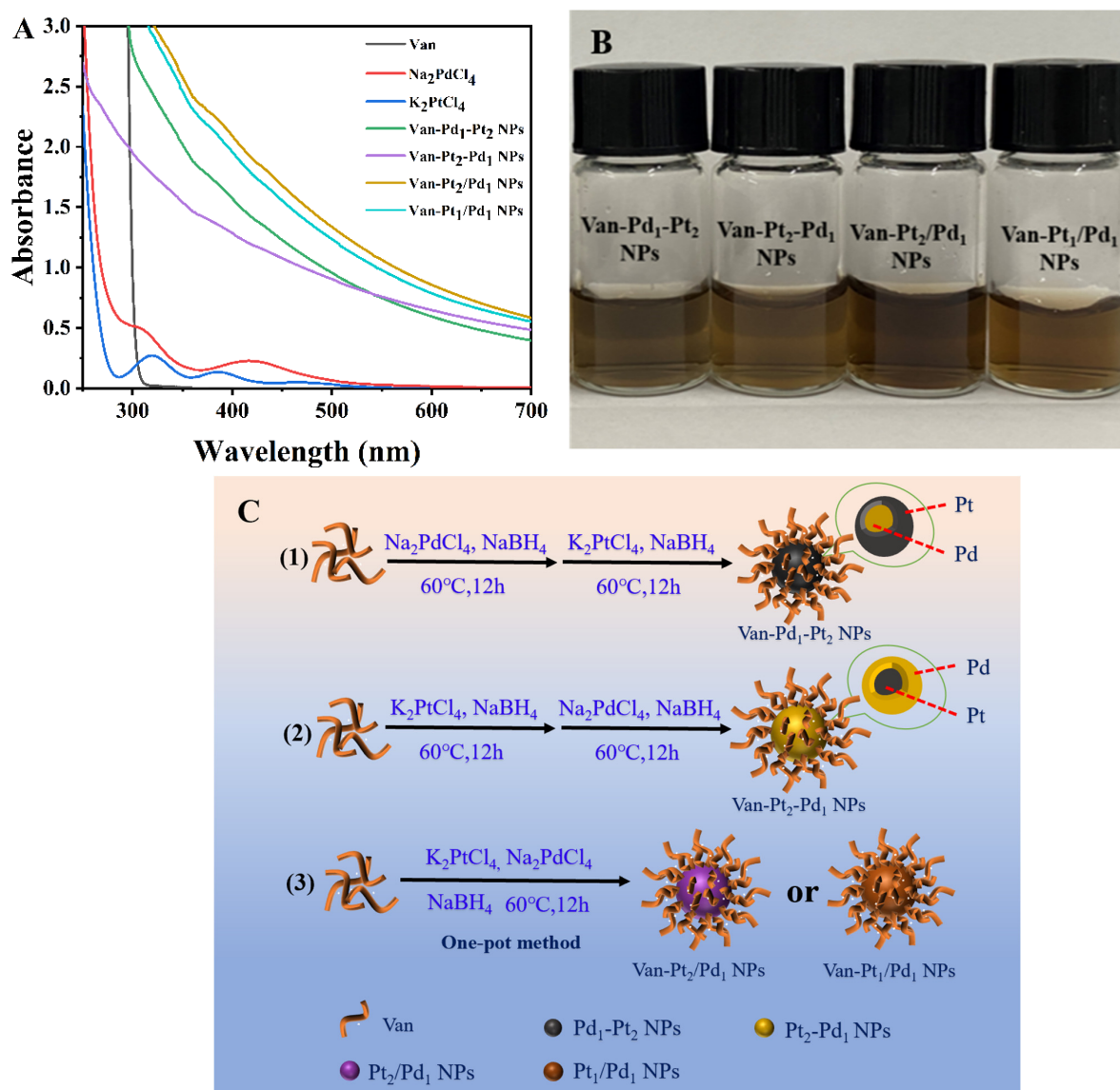


Figure 1. (A) UV-vis spectra of Van-Pt_m/Pd_n NPs. (B) Corresponding photographs of Van-Pt_m/Pd_n NPs and (C) schematic of the preparation of Van-Pt_m/Pd_n NPs ($m = 1, 2; n = 1, 2$).

As shown in Figure 2A–H, the particle sizes of the Van-Pd₁-Pt₂ NPs, Van-Pt₂-Pd₁ NPs, Van-Pt₂/Pd₁ NPs and Van-Pt₁/Pd₁ NPs were 5.3 ± 0.2 nm, 4.8 ± 0.6 nm, 5.7 ± 0.4 nm and 5.5 ± 0.5 nm, respectively. There was no significant difference in the particle size of the nanoparticles using the three synthesis methods. The Van-Pt₂-Pd₁ NPs and Van-Pd₁-Pt₂ NPs had a slight degree of aggregation. The Van-Pt₂/Pd₁ NPs and Van-Pt₁/Pd₁ NPs had better dispersion. The size of the Van-Pt_m/Pd_n NPs was very small. The aggregation of the Van-Pt₂-Pd₁ NPs and Van-Pd₁-Pt₂ NPs may be due to the long reaction time.

The catalytic reaction of the nanoparticles was carried out in aqueous solutions, the hydrodynamic size and zeta potential of nanoparticles affect their catalytic activity. As shown in Figure 3A, the hydrodynamic sizes of the Van-Pd₁-Pt₂ NPs, Van-Pt₂-Pd₁ NPs, Van-Pt₂/Pd₁ NPs and Van-Pt₁/Pd₁ NPs were 36.9 ± 4.1 nm, 34.2 ± 1.6 nm, 18.2 ± 1.0 nm and 16.1 ± 1.2 nm, respectively. They were slightly larger than those observed using TEM. The reason for this is that the water molecules form a thin water film around the nanoparticles in solution, resulting in a larger hydrodynamic size than that observed with TEM [35]. Compared with the Van-Pd₁-Pt₂ NPs and Van-Pt₂-Pd₁ NPs, the Van-Pt₂/Pd₁ NPs and Van-Pt₁/Pd₁ NPs prepared using the one-pot method exhibited a smaller hydrodynamic

size, which may be due to the dispersion performance of the Van-Pt₂/Pd₁ NPs and Van-Pt₁/Pd₁ NPs. In addition, the zeta potentials of the Van-Pt_m/Pd_n NPs were also determined (Figure 3B). The zeta potentials of the Van-Pd₁-Pt₂ NPs, Van-Pt₂-Pd₁ NPs, Van-Pt₂/Pd₁ NPs and Van-Pt₁/Pd₁ NPs in aqueous solution were -28.5 ± 2.1 mV, -29.5 ± 3.2 mV, -18.9 ± 2.5 mV and -20.6 ± 2.5 mV, respectively. The absolute values of the zeta potentials of all four nanoparticles were greater than 18 mV. Their zeta potential favored their good stability and maintenance of catalytic activity in the solution state.

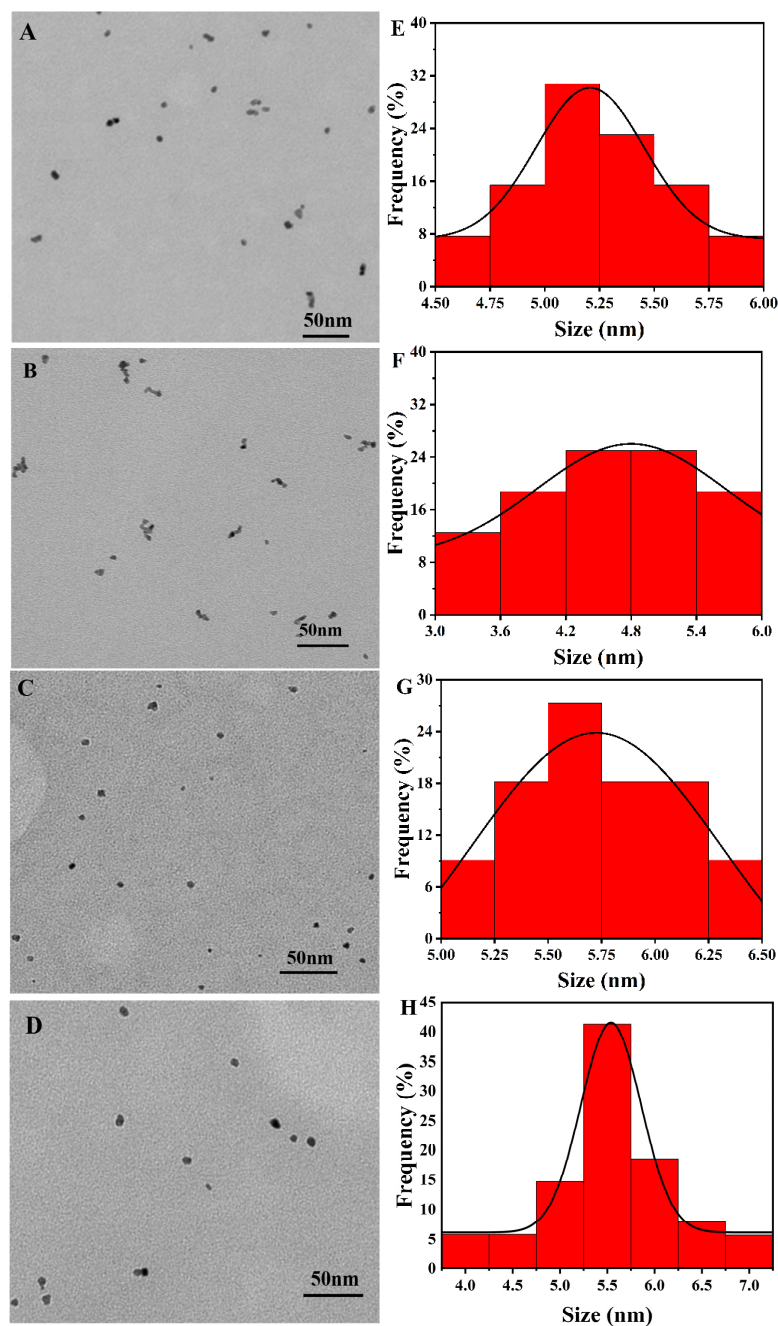


Figure 2. TEM images and size statistics of (A,E) Van-Pd₁-Pt₂ NPs, (B,F) Van-Pt₂-Pd₁ NPs, (C,G) Van-Pt₂/Pd₁ NPs and (D,H) Van-Pt₁/Pd₁ NPs.

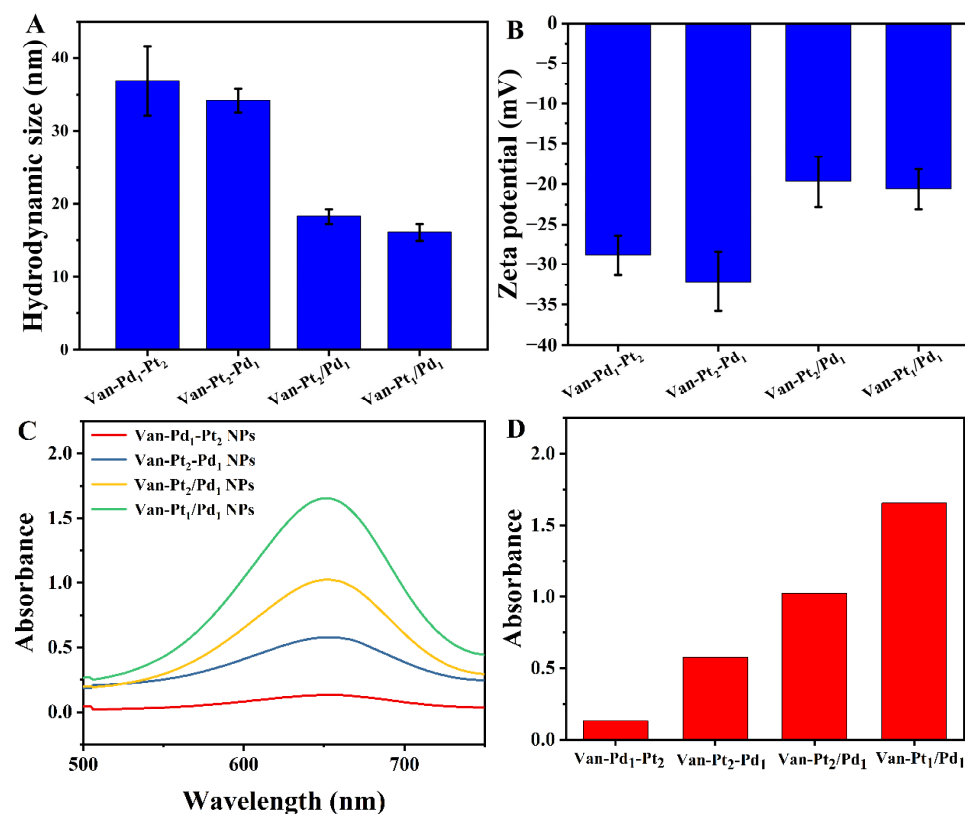


Figure 3. (A) Hydrodynamic size of Van-Pt_m/Pd_n NPs. (B) Zeta potential of Van-Pt_m/Pd_n NPs, (C) catalytic activities of Van-Pt_m/Pd_n NPs with different synthesis methods and (D) absorbance of (C) at 652 nm, ($m = 1, 2; n = 1, 2$), Van-Pt_m/Pd_n NPs reacted with TMB at 25 °C for 5 min.

The catalytic activity of nanozymes is also closely related to their preparation methods and reaction conditions. In order to obtain Van-Pt_m/Pd_n NPs with an excellent catalytic performance, we prepared nanoparticles with different metal ratios and different synthesis methods. Figure 3C shows that all the Van-Pt_m/Pd_n NPs had catalytic activity. Among them, the Van-Pt₁/Pd₁ NPs prepared using the one-pot method exhibited the highest catalytic ability for TMB oxidation. This indicated that the nanoparticles prepared using the one-pot method had good catalytic activity. In this case, the reaction time of the Van-Pt₁/Pd₁ NPs prepared using the one-pot method was 12 h, while the reaction time of the Van-Pt₁-Pd₁ NPs and Van-Pd₁-Pt₁ NPs prepared in a stepwise manner was 24 h, which caused the nanoparticles to become aggregated, leading to a decrease in the activity of the oxidase-like nanoparticles as compared to those obtained using the one-pot method. Meanwhile, we also compared other metal molar ratios of Van-Pt_m/Pd_n nanoparticles, i.e., $m:n = 1:1, 1:2, 2:1, 1:5, 5:1, 1:10$ and $10:1$, as shown in Figure S1. The results showed that the Van-Pt₁/Pd₁ NPs had the highest catalytic activity for TMB.

In short, among the three synthesis methods, the nanoparticles synthesized using the one-pot method had better dispersion and a smaller hydrodynamic size, which caused the nanoparticles to have more active sites; hence, the one-pot method was chosen to prepare the Pt Pd bimetallic nanoparticles. When comparing the catalytic activities of the nanozymes prepared with different molar ratios of Pt to Pd, the Van-Pt₁/Pd₁ NPs showed the highest catalytic activity; thus, we chose the Van-Pt₁/Pd₁ NPs for the subsequent experiments.

To further test our successful synthesis of Van-Pt_m/Pd_n NPs, we performed XPS and XRD characterizations of the Van-Pt₁/Pd₁ NPs. The XPS spectra of the Van-Pt₁/Pd₁ NPs showed five elements, C, N, O, Pt and Pd, as demonstrated in Figure 4A. Three elements, C, N and O, were derived from the biological template of Van, while Pt and Pd elements were reduced from K₂PtCl₄ and Na₂PdCl₄, respectively. The binding energies at 71.2 eV and

74.7 eV corresponded to the Pt 4f_{7/2} and Pt 4f_{5/2} orbitals of the Pt elements in Figure 4B, respectively [36]. This binding energy coincided with the binding energy of the 4f orbital of the Pt atom, which indicated that the Pt²⁺ in K₂PtCl₄ had been reduced to a Pt atom. In addition, the binding energies in Figure S2 are 284.6 eV, 286.2 eV and 288.6 eV, for which the corresponding chemical groups are C-C, C-O and C=O, respectively, and the C element was provided by Van [37–39]. Figure 4C shows the XPS spectrum of Pd 3d. The binding energies of 335.0 eV and 340.5 eV correspond to Pd 3d_{5/2} and Pd 3d_{3/2} orbitals, respectively, which were consistent with the 3d orbital binding energy of Pd at a valency of 0 in the Pt/Pd alloy [40]. Therefore, the successful loading of Pt/Pd alloy nanoparticles on the template of Van could be determined using XPS spectra, further proving our successful synthesis of Van-Pt₁/Pd₁ NPs. The XRD results showed that the diffraction peaks appeared at 39.76°, 46.24°, 67.45°, 81.28° and 85.71°, which correspond to the (1 1 1), (2 0 0), (2 2 0), (3 1 1) and (2 2 2) crystal planes of Pd and Pt, respectively (Figure 4D). Among the peaks, 39.76° and 46.24° are attributed to the planar crystal structure of Pt and Pd nanoparticles. Comparing the reference code 01-001-1194 for Pt and the reference pair 46–1043 for Pd, the diffraction peak is slightly higher than that of Pt and slightly lower than that of Pd. It is clear that the diffraction angles of the Van-Pt₁/Pd₁ NP alloy are in the middle of the diffraction peaks of Pt and Pd [41]. Thus, the XRD of the Pt-Pd alloy nanoparticles proved that we successfully synthesized Van-Pt₁/Pd₁ NPs using Van. The other peaks observed at 67.45°, 81.28° and 85.71° were related to the planar formation of Pt and Pd in the Van-Pt₁/Pd₁ NPs.

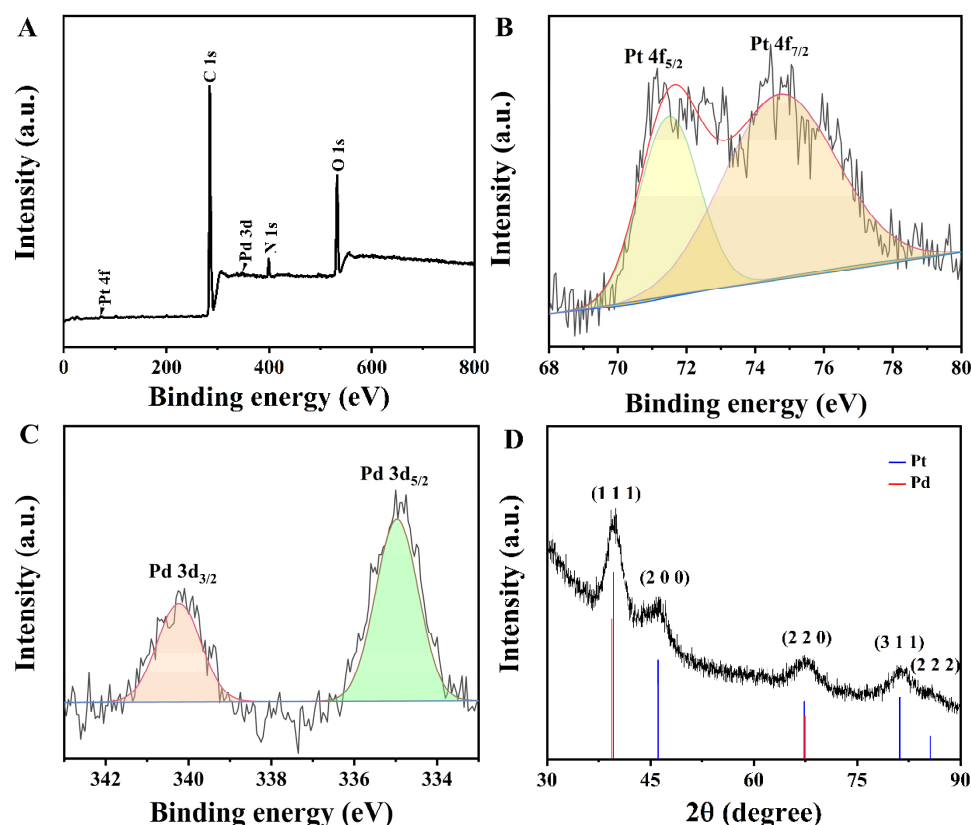


Figure 4. (A) XPS spectrum of Van-Pt₁/Pd₁ NPs, high-resolution XPS spectra of (B) Pt and (C) Pd, and (D) XRD spectrum of Van-Pt₁/Pd₁ NPs.

3.2. Catalytic Activity of Van-Pt₁/Pd₁ NPs

To test the catalytic activity of the Van-Pt₁/Pd₁ NPs, we designed the following groups: 1TMB, 2Van-Pt₁/Pd₁ NPs, 3TMB + Van-Pt₁/Pd₁ NPs and 4TMB + Pt₁/Pd₁ NPs. As shown in Figure 5A, the TMB + Van-Pt₁/Pd₁ NP group showed the highest characteristic absorption peak, and this characteristic absorption peak was provided by the oxidized TMB (oxTMB) [42,43]. During this experiment, the absorbance of the TMB and Van-Pt₁/Pd₁

NPs at 652 nm was close to 0, while the absorbance of the TMB + Pt₁/Pd₁ NP group was only 26% that of the TMB + Van-Pt₁/Pd₁ NPs group. Therefore, the oxidase-like activity originated from the synthesized Van-Pt₁/Pd₁ NPs.

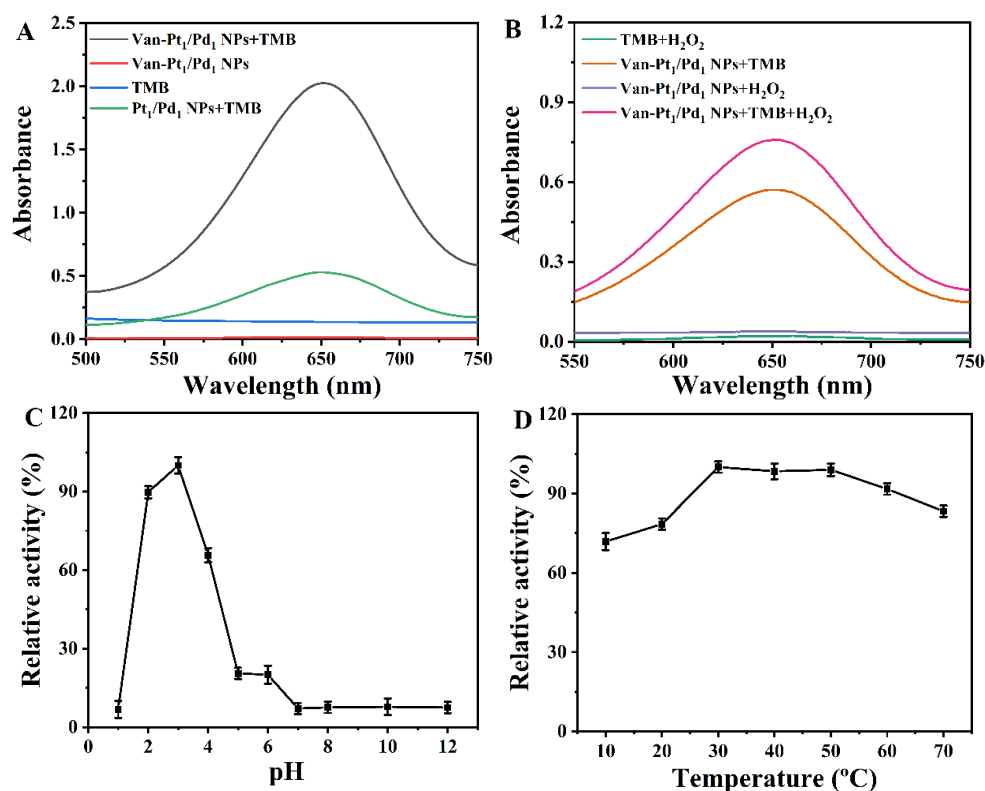


Figure 5. (A) Oxidase-like activity of Van-Pt₁/Pd₁ NPs with a reaction time of 5 min at 25 °C. (B) Peroxidase-like activity of Van-Pt₁/Pd₁ NPs with a reaction time of 2 min at 25 °C. (C) Optimal pH and (D) optimal temperature of Van-Pt₁/Pd₁ NPs.

We also designed different groups to investigate the peroxidase-like activity of Van-Pt₁/Pd₁ NPs: 1TMB + H₂O₂, 2Van-Pt₁/Pd₁ NPs + H₂O₂, 3TMB + Van-Pt₁/Pd₁ NPs and 4TMB + Van-Pt₁/Pd₁ NPs + H₂O₂. As shown in Figure 5B, the characteristic absorption peak of oxTMB at 652 nm was the highest in the Van-Pt₁/Pd₁ NPs + TMB + H₂O₂ group after 2 min of reaction. In addition, the TMB + H₂O₂ and Van-Pt₁/Pd₁ NPs + H₂O₂ groups did not show the characteristic absorption peak of oxTMB at 652 nm. Importantly, oxTMB peaks were observed in the TMB + Van-Pt₁/Pd₁ NP group under the influence of Van-Pt₁/Pd₁ NPs oxidase-like activity, but the absorbance was 25% lower than that of the TMB + Van-Pt₁/Pd₁ NPs + H₂O₂ group. Therefore, the Van-Pt₁/Pd₁ NPs had not only good oxidase-like activity but also peroxidase-like activity. The oxidase-like activity of the Van-Pt₁/Pd₁ NPs was very high; thus, the oxidase-like activity of the Van-Pt₁/Pd₁ NPs was investigated in the subsequent experiments.

The oxidase-like activity of Van-Pt₁/Pd₁ NPs is influenced by external conditions, the main influencing factors being pH and temperature. In order to find the optimal conditions for enzyme catalysis, the oxidase-like activity of the Van-Pt₁/Pd₁ NPs at different pHs and temperatures was investigated. From Figure 5C, it can be seen that the Van-Pt₁/Pd₁ NPs had the best oxidase-like activity at pH = 3. The oxidase-like activity of the Van-Pt₁/Pd₁ NPs decreased at other pHs. Therefore, the optimal pH for the oxidase-like activity of the Van-Pt₁/Pd₁ NPs was 3. The pH affects the binding of the TMB with the Van-Pt₁/Pd₁ NPs. The substrate TMB should not be suitable for binding to the Van-Pt₁/Pd₁ NPs at a non-optimal pH, leading to a decrease in oxidase-like activity. Furthermore, Van-Pt₁/Pd₁ NPs should have the highest amount of reactive oxygen species at pH = 3. The effect of temperature on the enzyme activity was then explored under the conditions of the optimal pH. In

Figure 5D, it can be seen that the highest value of the nanozymes' activity was reached at 30 °C. The activity of the nanozymes decreased at all other temperatures. However, the activity of the Van-Pt₁/Pd₁ NPs was maintained at a minimum of approximately 70%. Therefore, the optimal temperature for the Van-Pt₁/Pd₁ NPs was 30 °C, and they had a wide temperature range of catalytic performance. Thus, we can define the optimal conditions for the enzymatic activity of Van-Pt₁/Pd₁ NPs as pH = 3 and 30 °C. Subsequent experiments could be performed under these conditions. In addition, the catalytic activity of nanozymes is also related to nanoscale factors, such as their size, morphology and surface, which significantly affect their activity. Nayak et al. [44] assembled polyoxometalate (POM) (phosphotungstic acid (PTA)/phosphomolybdic acid (PMA)) nanoclusters and glucose oxidase (GOx) into microsphere structures, which facilitated the better diffusion of the reactants, intermediates and products due to the small size of the microspheres. This resulted in a 3–5-fold increase in the peroxidase-like activity of the PTA nanoclusters in the nanozyme microspheres.

To investigate the catalytic activity of the Van-Pt₁/Pd₁ NPs, the kinetic characterization of the nanozymes was required. The reaction kinetics of the nanozymes were determined by varying the concentration of the substrate TMB [32]. As shown in Figure 6A, the catalytic reaction followed the Michaelis–Menten equation in the concentration range of the substrate TMB (0.04–0.4 mM). As shown in Figure 6B, the standard equation was obtained as $y = 0.00899x + 0.04109$ ($R^2 = 0.999$) using the double-inverse data in Figure 6A. The K_m and V_{max} values of the Van-Pt₁/Pd₁ NPs were 0.218 mM and $24.337 \times 10^{-8} \text{ Ms}^{-1}$, respectively. It can be seen from Table 1 that the K_m of the Van-Pt₁/Pd₁ NPs was smaller compared to the other nano-enzymes, such as ZIF-67 (13.69 mM), PdPt₃-LNT NDs (0.263 mM), CeM (0.66 mM) and Cy-AuNCs (1.925 mM). Thus, the Van-Pt₁/Pd₁ NPs had an excellent affinity for TMB. In addition, the Van-Pt₁/Pd₁ NPs had a larger V_{max} ($24.337 \times 10^{-8} \text{ Ms}^{-1}$) compared to the other nanomaterials, including the PdPt₃-LNT NDs ($2.88 \times 10^{-8} \text{ Ms}^{-1}$), Pt-HMCN ($15.4 \times 10^{-8} \text{ Ms}^{-1}$), Pd₁₅₀-PCRNP NPs ($15.58 \times 10^{-8} \text{ Ms}^{-1}$) and N-CQDs ($4.49 \times 10^{-8} \text{ Ms}^{-1}$), which indicated that the Van-Pt₁/Pd₁ NPs had a better catalytic effect compared to monometallic materials and non-precious metals. Therefore, the Van-Pt₁/Pd₁ NPs had excellent oxidase-like activity, as shown not only by their larger V_{max} but also by their excellent affinity with TMB.

Table 1. Comparison of K_m and V_{max} .

| Materials | Substrate | K_m (mM) | V_{max} ($\times 10^{-8} \text{ Ms}^{-1}$) | Reference |
|--|-----------|------------|--|-----------|
| Van-Pt ₁ /Pd ₁ NPs | TMB | 0.218 | 24.337 | this work |
| PdPt ₃ -LNT NDs | TMB | 0.263 | 2.88 | [45] |
| Pt-HMCN | TMB | 0.124 | 15.4 | [46] |
| Pd ₁₅₀ -PCRNP NPs | TMB | 0.2 | 15.58 | [47] |
| N-CQDs | TMB | 0.515 | 4.49 | [48] |
| CeM | TMB | 0.66 | 1.71 | [49] |
| Cy-AuNCs | TMB | 1.925 | 212.3 | [50] |
| ZIF-67 | TMB | 13.69 | 31.96 | [51] |

Meanwhile, the oxidase-like activity of the Van-Pt₁/Pd₁ NPs was maintained at around 100% after one week of storage under ambient conditions, as shown in Figure 6C. Although the oxidase-like activity of the Van-Pt₁/Pd₁ NPs fluctuated to some extent, the variation was within the range of 98–102%. In addition, after 120 min of incubation in the temperature range of 10–90 °C, the catalytic performance of the Van-Pt₁/Pd₁ NPs remained around 90% in the range of 70–90 °C, as shown in Figure 6D. These findings indicated that the Van-Pt₁/Pd₁ NPs had good stability in different pH conditions and temperature tolerance, and they had good catalytic activity in extreme environments.

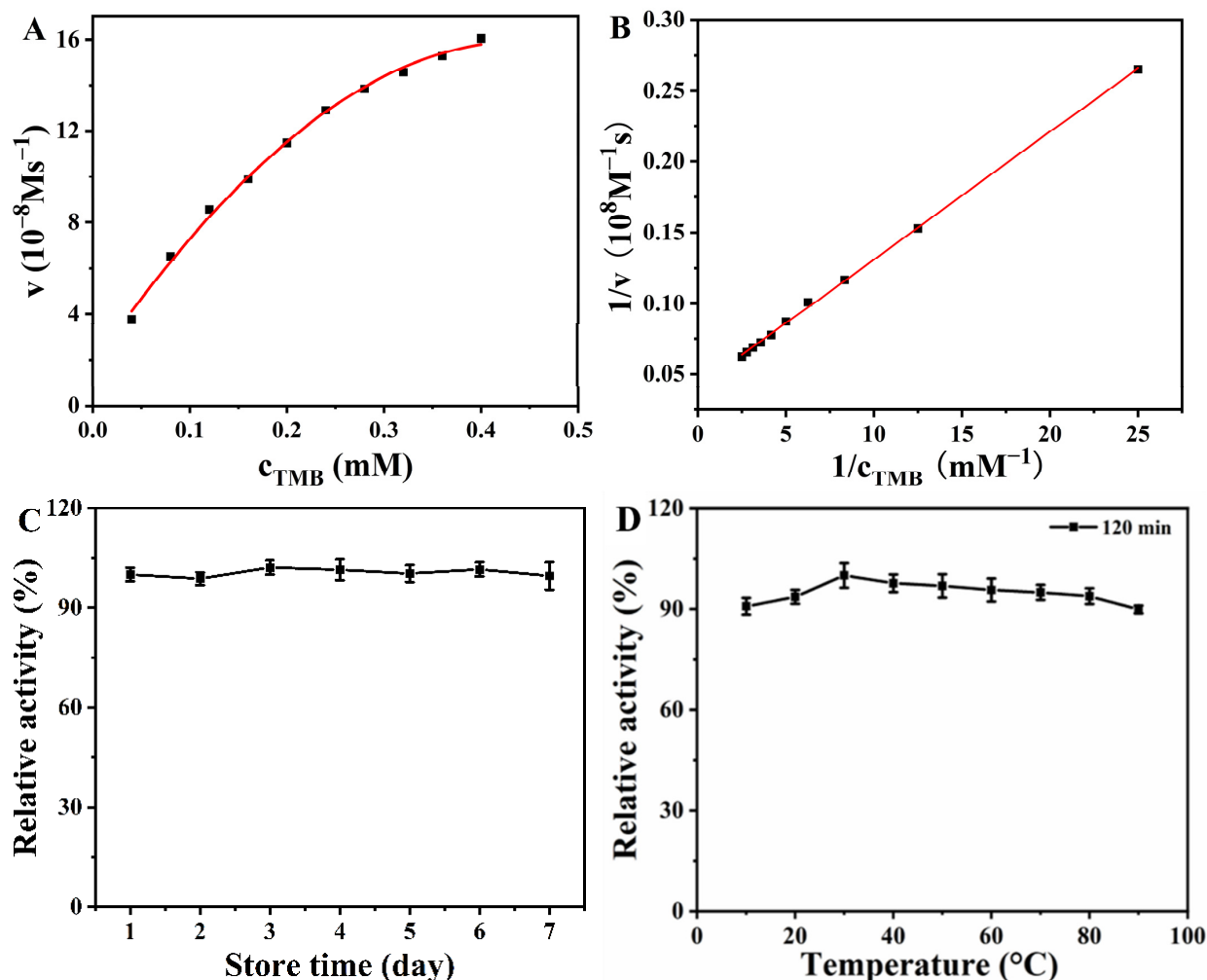


Figure 6. (A) Catalytic kinetic diagram of different TMB concentrations. (B) is the double-inverse curve of (A). (C) The seven-day stability of the Van-Pt₁/Pd₁ NPs and (D) the stability of the Van-Pt₁/Pd₁ NPs at different temperatures. Van-Pt₁/Pd₁ NPs were incubated at different temperature for 2 h.

3.3. Mechanism of the Oxidase-Like Activity of Van- Pt₁/Pd₁ NPs

The oxidation reaction of TMB based on Van-Pt₁/Pd₁ NPs is closely related to reactive oxygen species [20]. Reactive oxygen species include as singlet oxygen ($^1\text{O}_2$), hydroxyl radical ($\cdot\text{OH}$), superoxide anion ($\text{O}_2^{\cdot-}$), etc. The mechanism of the oxidase-like activity of Van-Pt₁/Pd₁ NPs was investigated by adding different reactive oxygen species inhibitors, such as BQ, NaN_3 and IPA, which have quenching effects on $\text{O}_2^{\cdot-}$, $^1\text{O}_2$ and $\cdot\text{OH}$, respectively.

To investigate the mechanism of the oxidase-like activity of Van-Pt₁/Pd₁ NPs, different experimental groups were set up, as shown in Figure 7A. It showed that the addition of NaN_3 into the Van-Pt₁/Pd₁ NPs + TMB system (36%) had the greatest effect on the absorbance of the reaction, followed by the effect of IPA (77%), while BQ (104%) had the least effect and showed almost no difference compared with the control group of Van-Pt₁/Pd₁ NPs + TMB (100%). Therefore, the type of reactive oxygen species produced by the Van-Pt₁/Pd₁ NPs with oxidase-like activity was mainly $^1\text{O}_2$, containing a small amount of $\cdot\text{OH}$ with no $\text{O}_2^{\cdot-}$ production.

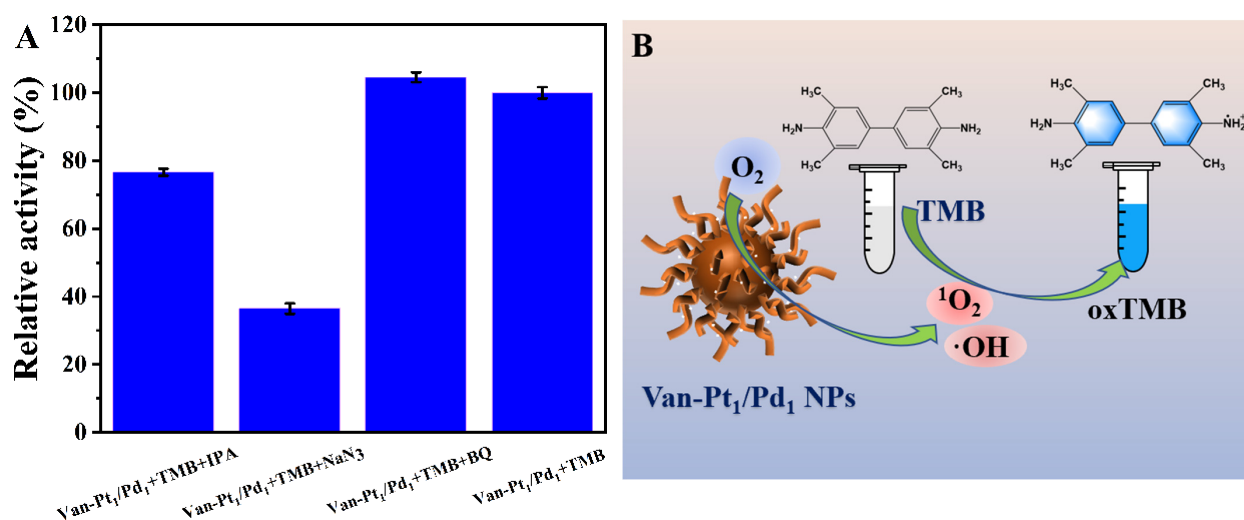


Figure 7. (A) Mechanism of oxidase-like activity and (B) catalytic process of Van-Pt₁/Pd₁ NPs. The reaction was at 30 °C, pH = 3, for 5 min. BQ, NaN₃ and IPA had suppressive effects on O₂⁻, ¹O₂ and [•]OH, respectively.

3.4. L-cysteine Assay

Here, the cytotoxicity of the Van-Pt₁/Pd₁ NPs and Van was explored using the MTT assay. As shown in Figure 8A, when the concentration of the Van-Pt₁/Pd₁ NPs and Van was 200 µg/mL, the cell viability was maintained above 90%. This indicated that the Van-Pt₁/Pd₁ NPs were non-cytotoxic, as compared to previously reported Pt NPs and Pd NPs [52]. Therefore, the Van-Pt₁/Pd₁ NPs synthesized using the bio-template method have good biocompatibility. As shown in Figure 8B, L-cysteine is a reducing biomass that can reduce oxTMB to TMB. Therefore, we could use the excellent oxidase-like activity of Van-Pt₁/Pd₁ NPs to establish a standard curve for the L-cysteine assay. The experimental system included Van-Pt₁/Pd₁ NPs, TMB and L-cysteine. The UV-vis spectrum of the solution was detected using a UV-vis spectrophotometer. As shown in Figure 8C, the calibration showed a good linear relationship with the absorbance value at 652 nm. The standard detection equation of the Van-Pt₁/Pd₁ NPs for L-cysteine was $Y = 0.379 + 15.367 \times C_{\text{L-cysteine}}$ ($R^2 = 0.997$), while the corresponding detection range of the L-cysteine concentration was 6–100 µM, and the detection limit was 0.0703 µM. Table 2 shows a comparison of the detection ranges and detection limits of L-cysteine for different materials. The Van-Pt₁/Pd₁ NPs (6–100 µM) had a wider linear range than the other sensors, including the MoS₂-Au@Pt (0.8–54.4 µM), SPB@Pt NPs (0.4–3.5 µM) and Au-Ag (0.075–2 µM). In addition, Van-Pt₁/Pd₁ NPs had a lower detection limit (0.07 µM) than other sensors, such as PdPt₃-LNT NDs (3.10 µM), Cu@Au/Pt (4.00 µM), VS₄ NPs (2.50 µM) and CuMnO₂ NFs (11.26 µM). Therefore, the colorimetric method had a wide linear detection range and a low sensitivity detection limit.

Table 2. Comparison of L-cysteine detection range and detection limit for different materials.

| Materials | Detection Method | Linear Range (µM) | LOD (µM) | Reference |
|--|------------------|-------------------|----------|-----------|
| Van-Pt ₁ /Pd ₁ NPs | Colorimetry | 6–100 | 0.07 | this work |
| PdPt ₃ -LNT NDs | Colorimetry | 0–200 | 3.10 | [45] |
| MoS ₂ -Au@Pt | Colorimetry | 0.8–54.4 | 0.50 | [53] |

Table 2. Cont.

| Materials | Detection Method | Linear Range (μM) | LOD (μM) | Reference |
|---------------------------------------|------------------|--------------------------------|-----------------------|-----------|
| SPB@Pt NPs | Colorimetry | 0.4–3.5 | 0.11 | [54] |
| Cu@Au/Pt | Colorimetry | 0–400 | 4.00 | [55] |
| VS ₄ NPs | Colorimetry | 5–100 | 2.50 | [56] |
| CuMnO ₂ NFs | Colorimetry | 20–300 | 11.26 | [57] |
| OV-Mn ₃ O ₄ NFs | Colorimetry | 5–800 | 1.31 | [58] |
| Ag NPs | Colorimetry | 0.001–1 | 0.001 | [59] |
| silver NPs | Colorimetry | 1.5–6 | 0.05 | [60] |
| QX-AgNPs | Colorimetry | 10–60 | 0.0027 | [61] |
| PQDs | Fluorescence | 0–800 | 28.11 | [62] |
| Au-Ag | Fluorescence | 0.075–2 | 0.04 | [63] |
| oPAD | Electrochemical | 10–800 | 5.50 | [64] |

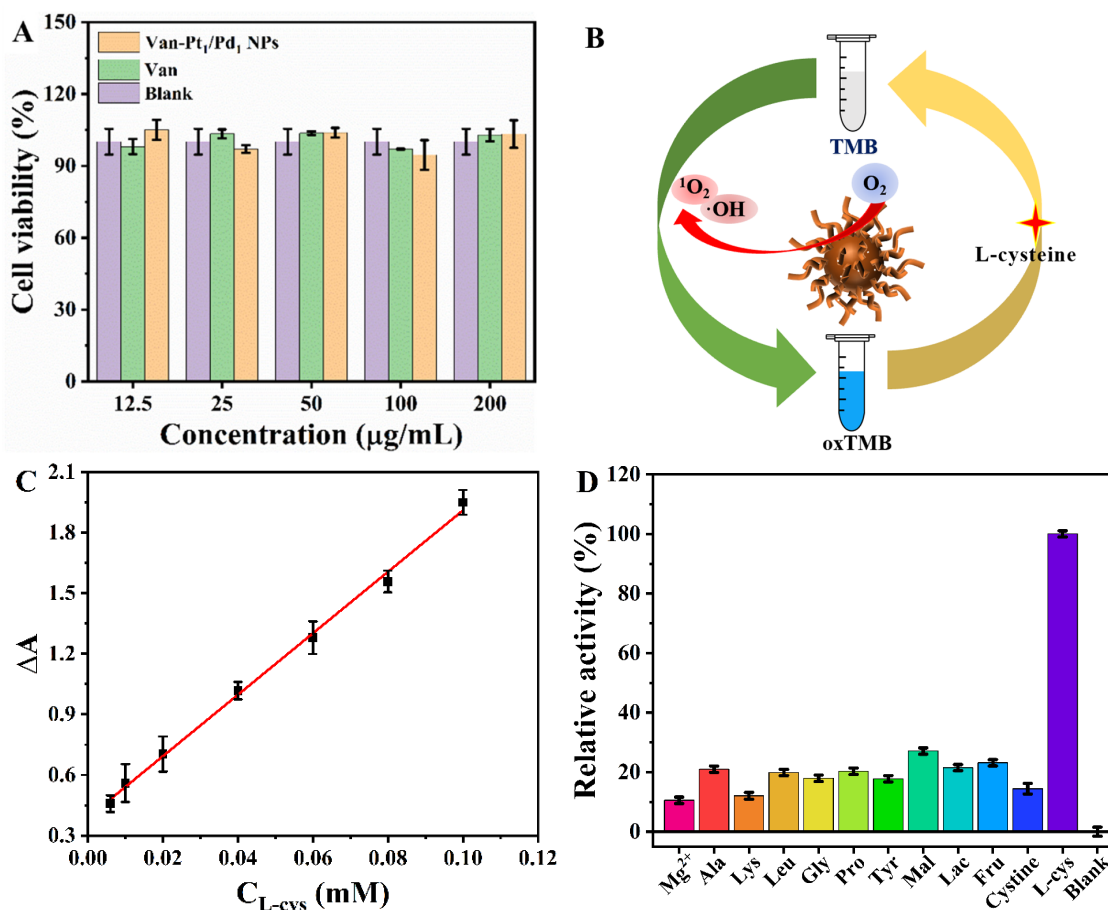


Figure 8. (A) Biocompatibility of Van-Pt₁/Pd₁ NPs. (B) Schematic diagram of Van-Pt₁/Pd₁ NPs for L-cysteine detection. (C) Linear fit of ΔA for L-cysteine in the concentration range of 6–100 μM and (D) selectivity of Van-Pt₁/Pd₁ NPs.

The selectivity of the Van-Pt₁/Pd₁ NPs was investigated by detecting L-cysteine (L-cys) and potentially interfering substances, such as Mg²⁺, alanine (Ala), phenylalanine (Phe), leucine (Leu), glycine (Gly), proline (Pro), glutamic acid (Glu), maltose (Mal), lactose (Lac) and fructose (Fru). As shown in Figure 8D, the absorbance of L-cysteine was much higher than that of the other interfering agents, even when the concentration of interfering agents was three times higher than that of L-cysteine. This indicated that the Van-Pt₁/Pd₁ NPs had good selectivity as probes for detecting L-cysteine. The selectivity of the Van-Pt₁/Pd₁ NPs for L-cysteine was high and reasonable, as compared with other reports [58,62].

To assess the potential for, and feasibility of, application in practical assays, different L-cysteine levels in mouse serum were monitored using a standard addition method. As shown in Table 3, the recoveries are 98.8% and 105.6%, respectively, indicating that the nanozymes can be applied in real samples. The good detection performance of Van-Pt₁/Pd₁ NPs may be related to the smaller particle size and better stability of the nanoparticles.

Table 3. Recovery of L-cysteine assay in different samples.

| Sample | Added L-cysteine Concentration (μM) | Found L-cysteine Concentration (μM) | Recovery (%) | RSD (%) |
|-------------|-------------------------------------|-------------------------------------|--------------|---------|
| Mouse serum | 50 | 52.1 | 100.2 | 0.57 |
| | 90 | 90.1 | 102.8 | 1.11 |

4. Conclusions

In conclusion, we successfully synthesized a Van-Pt₁/Pd₁ NP bimetallic nanozyme with good oxidase-like activity and peroxidase-like activity by exploring the synthesis methods and metal ratios. The catalytic kinetics of the Van-Pt₁/Pd₁ NPs was in accordance with the typical Michaelis–Menten equation, and the smaller K_m proved that the Van-Pt₁/Pd₁ NPs had a good affinity for TMB. The Van-Pt₁/Pd₁ NPs had a good storage stability. Meanwhile, the Van-Pt₁/Pd₁ NPs were almost non-cytotoxic, as measured using the MTT assay. More importantly, a simple, fast and reliable L-cysteine assay was established using the prepared Van-Pt₁/Pd₁ NPs with a wide detection range of 6–100 μM and a low detection limit of 0.07 μM. In conclusion, stable Van-Pt₁/Pd₁ NPs were synthesized successfully and could be applied in the field of biomass detection.

Supplementary Materials: The following supporting information can be downloaded at: <https://www.mdpi.com/article/10.3390/biom13081254/s1>, Figure S1: Oxidase-like activity of Van-Pt_m/Pd_n NPs with different ratios of Pt and Pd at 652 nm; Figure S2: High-resolution XPS spectrum of C; Figure S3: Infrared spectra of Van and Van-Pt₁/Pd₁ NPs.

Author Contributions: H.Z.: investigation, writing—original draft. K.L.: investigation. L.Z.: formal analysis. T.Z.: data curation. L.W.: supervision, writing—review and editing. X.J.: writing—review and editing. Y.C.: methodology, writing—review and editing. Z.H.: conceptualization, writing—review and editing. J.H.: methodology. G.M.: writing—review and editing. All authors have read and agreed to the published version of the manuscript.

Funding: This research was funded by the Science and Technology Project of Hebei Education Department (QN2022124), Natural Science Foundation of Hebei Province (B2017203229, H2022203004), Key Program of Hebei University of Environmental Engineering (2020ZRZD02), and Yanshan University's Speciality (Medical Engineering Interdisciplinarity) Cultivation Project (UH202209).

Institutional Review Board Statement: Not applicable.

Informed Consent Statement: Not applicable.

Data Availability Statement: The data presented in this study are available on request from the corresponding author.

Conflicts of Interest: The authors declare no conflict of interest.

References

- Ge, C.; Shen, F.; Yin, Y.; Zhou, P.; Lu, C. A novel near-infrared and naked-eye fluorescence probe with a large stokes shift for specific detection of cysteine and its application in living cells. *Tetrahedron Lett.* **2020**, *61*, 151963. [CrossRef]
- Prasetia, R.; Fuangswasdi, S.; Unob, F. Silver nanoparticle-supported hydroxyapatite as a material for visual detection of urinary cysteine. *Anal. Methods* **2019**, *11*, 2888–2894. [CrossRef]
- Dizman, H.M.; Kazancioglu, E.O.; Shigemune, T.; Takahara, S.; Arsu, N. High sensitivity colorimetric determination of L-cysteine using gold nanoparticles functionalized graphene oxide prepared by photochemical reduction method. *Spectrochim. Acta A Mol. Biomol. Spectrosc.* **2022**, *264*, 120294. [CrossRef]

4. Feng, S.; Wen, F.; He, L.; Su, J.; Jiang, P.; He, D. Facile synthesis of ultrathin MnO₂ nanobelts anchoring on porous carbon with high oxidase mimetic activity for L-cysteine colorimetric detection. *Sensor. Actuat. B-Chem.* **2022**, *361*, 131745. [[CrossRef](#)]
5. Zhang, H.; Yue, X.; Li, W.; Chen, W.; Wang, Y.; Li, X.; Ye, Y.; Song, X. Selective and discriminative fluorescence sensing of Cys, Hcy, GSH and H₂S with concise and distinct signals. *Sensor. Actuat. B-Chem.* **2021**, *331*, 129394. [[CrossRef](#)]
6. Zhuge, W.; Liu, Y.; Huang, W.; Zhang, C.; Wei, L.; Peng, J. Conductive 2D phthalocyanine-based metal-organic framework as a photoelectrochemical sensor for N-acetyl-L-cysteine detection. *Sensor. Actuat. B-Chem.* **2022**, *367*, 132028. [[CrossRef](#)]
7. Liu, C.; Zhao, Y.; Xu, D.; Zheng, X.; Huang, Q. A green and facile approach to a graphene-based peroxidase-like nanozyme and its application in sensitive colorimetric detection of l-cysteine. *Anal. Bioanal. Chem.* **2021**, *413*, 4013–4022. [[CrossRef](#)]
8. Huang, Z.; Yang, Y.; Long, Y.; Zheng, H. A colorimetric method for cysteine determination based on the peroxidase-like activity of ficin. *Anal. Methods* **2018**, *10*, 2676–2680. [[CrossRef](#)]
9. Gao, L.; Zhuang, J.; Nie, L.; Zhang, J.; Zhang, Y.; Gu, N.; Wang, T.; Feng, J.; Yang, D.; Perrett, S.; et al. Intrinsic peroxidase-like activity of ferromagnetic nanoparticles. *Nat. Nanotechnol.* **2007**, *2*, 577–583. [[CrossRef](#)]
10. Liu, K.; Zhao, Y.; Zhang, L.; He, M.; Lin, W.; Sun, H.; Liu, Z.; Hu, J.; Wang, L. Biocompatible Platinum nanoclusters prepared using bitter melon polysaccharide for colorimetric detection of ascorbic acid. *Biomolecules* **2021**, *11*, 647. [[CrossRef](#)]
11. Magesa, F.; Wu, Y.; Dong, S.; Tian, Y.; Li, G.; Vianney, J.M.; Buza, J.; Liu, J.; He, Q. Electrochemical sensing fabricated with Ta₂O₅ nanoparticle-electrochemically reduced graphene oxide nanocomposite for the detection of oxytetracycline. *Biomolecules* **2020**, *10*, 110. [[CrossRef](#)] [[PubMed](#)]
12. Majumder, S.; Ranjan Dahiya, U.; Yadav, S.; Sharma, P.; Ghosh, D.; Rao, G.K.; Rawat, V.; Kumar, G.; Kumar, A.; Srivastava, C.M. Zinc oxide nanoparticles functionalized on hydrogel grafted silk fibroin fabrics as efficient composite dressing. *Biomolecules* **2020**, *10*, 1117. [[CrossRef](#)] [[PubMed](#)]
13. Liang, C.; Lan, Y.; Sun, Z.; Zhou, L.; Li, Y.; Liang, X.; Qin, X. Synthesis of carbon quantum dots with iron and nitrogen from Passiflora edulis and their peroxidase-mimicking activity for colorimetric determination of uric acid. *Microchim. Acta* **2020**, *187*, 405. [[CrossRef](#)] [[PubMed](#)]
14. Sun, W.; Wang, N.; Zhou, X.; Sheng, Y.; Su, X. Co, N co-doped porous carbon-based nanozyme as an oxidase mimic for fluorescence and colorimetric biosensing of butyrylcholinesterase activity. *Microchim. Acta* **2022**, *189*, 363. [[CrossRef](#)]
15. Gao, L.-Z.; Yan, X.-Y. Discovery and Current Application of Nanozyme. *Prog. Biochem. Biophys.* **2013**, *40*, 892–902. [[CrossRef](#)]
16. Lai, X.; Shen, Y.; Gao, S.; Chen, Y.; Cui, Y.; Ning, D.; Ji, X.; Liu, Z.; Wang, L. The Mn-modified porphyrin metal-organic framework with enhanced oxidase-like activity for sensitively colorimetric detection of glutathione. *Biosens. Bioelectron.* **2022**, *213*, 114446. [[CrossRef](#)] [[PubMed](#)]
17. Ramasamy, M.; Nanda, S.S.; Lee, J.-H.; Lee, J. Construction of alizarin conjugated graphene oxide composites for inhibition of candida albicans biofilms. *Biomolecules* **2020**, *10*, 565. [[CrossRef](#)] [[PubMed](#)]
18. Sanchez-Rodriguez, C.; Palao-Suay, R.; Rodriganez, L.; Rosa Aguilar, M.; Martin-Saldana, S.; San Roman, J.; Sanz-Fernandez, R. alpha-Tocopheryl succinate-based polymeric nanoparticles for the treatment of head and neck squamous cell carcinoma. *Biomolecules* **2018**, *8*, 97. [[CrossRef](#)]
19. Pandey, P.C.; Mitra, M.D.; Shukla, S.; Narayan, R.J. Organotrialkoxysilane-functionalized noble metal monometallic, bimetallic, and trimetallic nanoparticle mediated non-enzymatic sensing of glucose by resonance rayleigh scattering. *Biosens.-Basel* **2021**, *11*, 122. [[CrossRef](#)]
20. Maksimchuk, P.O.; Hubenko, K.O.; Seminko, V.V.; Karbivskii, V.L.; Tkachenko, A.S.; Onishchenko, A.I.; Prokopyuk, V.Y.; Yefimova, S.L. High antioxidant activity of gadolinium-yttrium orthovanadate nanoparticles in cell-free and biological milieu. *Nanotechnology* **2022**, *33*, 055701. [[CrossRef](#)]
21. Li, R.; Fan, L.; Chen, S.; Wang, L.; Cui, Y.; Ma, G.; Zhang, X.; Liu, Z. Zwitterionic sulfhydryl sulfobetaine stabilized platinum nanoparticles for enhanced dopamine detection and antitumor ability. *ACS Appl. Mater.* **2022**, *14*, 55201–55216. [[CrossRef](#)] [[PubMed](#)]
22. Tan, F.; Xie, X.; Xu, A.; Deng, K.; Zeng, Y.; Yang, X.; Huang, H. Fabricating and regulating peroxidase-like activity of eggshell membrane-templated gold nanoclusters for colorimetric detection of staphylococcal enterotoxin B. *Talanta* **2019**, *194*, 634–642. [[CrossRef](#)]
23. Sun, H.; Lv, Y.; Zhang, J.; Zhou, C.; Su, X. A dual-signal fluorometric and colorimetric sensing platform based on gold-platinum bimetallic nanoclusters for the determination of beta-galactosidase activity. *Anal. Chim. Acta* **2023**, *1252*, 341010. [[CrossRef](#)] [[PubMed](#)]
24. Ma, L.; Zhang, Q.; Wu, C.; Zhang, Y.; Zeng, L. PtNi bimetallic nanoparticles loaded MoS₂ nanosheets: Preparation and electrochemical sensing application for the detection of dopamine and uric acid. *Anal. Chim. Acta* **2019**, *1055*, 17–25. [[CrossRef](#)] [[PubMed](#)]
25. Jang, M.-H.; Kizilkaya, O.; Kropf, A.J.; Kurtz, R.L.; Elam, J.W.; Lei, Y. Synergetic effect on catalytic activity and charge transfer in Pt-Pd bimetallic model catalysts prepared by atomic layer deposition. *J. Chem. Phys.* **2020**, *152*, 024710. [[CrossRef](#)] [[PubMed](#)]
26. Jin, L.; Sun, Y.; Shi, L.; Li, C.; Shen, Y. PdPt bimetallic nanowires with efficient oxidase mimic activity for the colorimetric detection of acid phosphatase in acidic media. *J. Mater. Chem. B.* **2019**, *7*, 4561–4567. [[CrossRef](#)]
27. Li, R.; Zhao, Y.; Zhang, T.; Ju, Z.; Ji, X.; Cui, Y.; Wang, L.; Xiao, H. Pd nanoparticles stabilized by bitter melon polysaccharide with peroxidase properties for H₂O₂ detection. *Int. J. Biol. Macromol.* **2023**, *233*, 123513. [[CrossRef](#)] [[PubMed](#)]

28. Kalantari, M.; Ghosh, T.; Liu, Y.; Zhang, J.; Zou, J.; Lei, C.; Yu, C. Highly thiolated dendritic mesoporous silica nanoparticles with high-content gold as nanozymes: The nano-gold size matters. *ACS Appl. Mater.* **2019**, *11*, 13264–13272. [[CrossRef](#)]
29. Zha, J.; Wu, W.; Xie, P.; Han, H.; Fang, Z.; Chen, Y.; Jia, Z. Polymeric nanocapsule enhances the peroxidase-like activity of Fe₃O₄ nanozyme for removing organic dyes. *Catalysts* **2022**, *12*, 614. [[CrossRef](#)]
30. Dong, L.; Li, R.; Wang, L.; Lan, X.; Sun, H.; Zhao, Y.; Wang, L. Green synthesis of platinum nanoclusters using lentinan for sensitively colorimetric detection of glucose. *Int. J. Biol. Macromol.* **2021**, *172*, 289–298. [[CrossRef](#)]
31. Retout, M.; Gosselin, B.; Mattiuzzi, A.; Ternad, I.; Jabin, I.; Bruylants, G. Peptide-conjugated silver nanoparticles for the colorimetric detection of the oncoprotein Mdm2 in human serum. *Chempluschem* **2022**, *87*, e202100450. [[CrossRef](#)] [[PubMed](#)]
32. Dong, J. On catalytic kinetics of enzymes. *Processes* **2021**, *9*, 271. [[CrossRef](#)]
33. Chen, J.; Lu, Y.; Yan, F.; Wu, Y.; Huang, D.; Weng, Z. A fluorescent biosensor based on catalytic activity of platinum nanoparticles for freshness evaluation of aquatic products. *Food Chem.* **2020**, *310*, 125922. [[CrossRef](#)] [[PubMed](#)]
34. Velidandi, A.; Sarvepalli, M.; Pabbathi, N.P.P.; Baadhe, R.R. Biogenic synthesis of novel platinum-palladium bimetallic nanoparticles from aqueous *Annona muricata* leaf extract for catalytic activity. *3 Biotech* **2021**, *11*, 385. [[CrossRef](#)] [[PubMed](#)]
35. Zhang, L.; Guo, Q.; Zheng, R.; Yu, Q.; Liang, Y.; Ma, G.; Li, Q.; Zhang, X.; Xiao, H.; Wang, L. Zwitterionic targeting doxorubicin-loaded micelles assembled by amphiphilic dendrimers with enhanced antitumor performance. *Langmuir* **2023**, *39*, 4766–4776. [[CrossRef](#)] [[PubMed](#)]
36. Wang, R.; Feng, J.-J.; Xue, Y.; Wu, L.; Wang, A.-J. A label-free electrochemical immunosensor based on AgPt nanorings supported on reduced graphene oxide for ultrasensitive analysis of tumor marker. *Sensor. Actuat. B-Chem.* **2018**, *254*, 1174–1181. [[CrossRef](#)]
37. Geng, W.; Kumabe, Y.; Nakajima, T.; Takanashi, H.; Ohki, A. Analysis of hydrothermally-treated and weathered coals by X-ray photoelectron spectroscopy (XPS). *Fuel* **2009**, *88*, 644–649. [[CrossRef](#)]
38. Jia, L.; Zhang, J.; Su, G.; Zheng, Z.; Zhou, T. Locally controllable surface foaming of polymers induced by graphene via near-infrared pulsed laser. *ACS Sustain. Chem. Eng.* **2020**, *8*, 2498–2511. [[CrossRef](#)]
39. Rocky, B.P.; Thompson, A.J. Analyses of the chemical compositions and structures of four bamboo species and their natural fibers by infrared, laser, and X-ray spectroscopies. *Fiber Polym.* **2021**, *22*, 916–927. [[CrossRef](#)]
40. Dong, F.; Yamazaki, K. The Pt-Pd alloy catalyst and enhanced catalytic activity for diesel oxidation. *Catal. Today* **2021**, *376*, 47–54. [[CrossRef](#)]
41. Deng, L.; Xu, Q.; Rao, L.; Yue, R.; Xu, J.; Duan, X. Preparation of hierarchical Pt/Pd-PEDOT/NGE nanocomposites for high caffeic acid electrochemical sensing performance. *J. Electron. Mater.* **2021**, *50*, 543–553. [[CrossRef](#)]
42. Alam, N.; Ravikumar, C.H.; Sreeramareddy, M.; Somasundrum, M.; Surareungchai, W. Label-free ultra-sensitive colorimetric detection of hepatitis E virus based on oxidase-like activity of MnO₂ nanosheets. *Anal. Bioanal. Chem.* **2022**, *415*, 703–713. [[CrossRef](#)] [[PubMed](#)]
43. Chen, T.; Cao, J.; Bao, X.; Peng, Y.; Liu, L.; Fu, W. Co nanoparticles decorated with N-doped carbon nanotubes as high-efficiency catalysts with intrinsic oxidase-like property for colorimetric sensing. *RSC Adv.* **2021**, *11*, 39966–39977. [[CrossRef](#)] [[PubMed](#)]
44. Nayak, J.; Chilivery, R.; Kumar, A.K.; Begum, G.; Rana, R.K. A bioinspired assembly to simultaneously heterogenize polyoxometalates as nanozymes and encapsulate enzymes in a microstructure endowing efficient peroxidase-mimicking activity. *ACS Sustain. Chem. Eng.* **2021**, *9*, 15819–15829. [[CrossRef](#)]
45. Ma, Z.; Dong, L.; Zhang, B.; Liang, B.; Wang, L.; Ma, G.; Wang, L. Lentinan stabilized bimetallic PdPt₃ dendritic nanoparticles with enhanced oxidase-like property for L-cysteine detection. *Int. J. Biol. Macromol.* **2022**, *216*, 779–788. [[CrossRef](#)] [[PubMed](#)]
46. Chen, H.; Yuan, C.; Yang, X.; Cheng, X.; Elzatahry, A.A.; Alghamdi, A.; Su, J.; He, X.; Deng, Y. Hollow mesoporous carbon nanospheres loaded with Pt nanoparticles for colorimetric detection of ascorbic acid and dluose. *ACS Appl. Nano Mater.* **2020**, *3*, 4586–4598. [[CrossRef](#)]
47. Li, S.; Zhao, Y.; Ji, F.; Zheng, R.; Ji, X.; Liu, Z.; Wang, L. Biocompatible pericarpium citri reticulatae polysaccharide templated Pd nanoparticles for effectively colorimetric detection of glutathione. *Colloid. Surface. A* **2022**, *650*, 129617. [[CrossRef](#)]
48. Yadav, P.K.; Singh, V.K.; Chandra, S.; Bano, D.; Kumar, V.; Talat, M.; Hasan, S.H. Green synthesis of fluorescent carbon quantum dots from *azadirachta indica* leaves and their peroxidase-mimetic activity for the detection of H₂O₂ and ascorbic acid in common fresh fruits. *ACS Biomater. Sci. Eng.* **2019**, *5*, 623–632. [[CrossRef](#)]
49. Singh, G.; Kushwaha, A.; Sharma, M. Persistent peroxidase mimics of graphene oxide anchored cerium molybdate sensor: An effective colorimetric detection of S²⁻ and Sn²⁺ ions. *Microchem. J.* **2020**, *153*, 104290. [[CrossRef](#)]
50. Jiang, C.; Zhang, C.; Song, J.; Ji, X.; Wang, W. Cytidine-gold nanoclusters as peroxidase mimetic for colorimetric detection of glutathione (GSH), glutathione disulfide (GSSG) and glutathione reductase (GR). *Spectrochim. Acta A Mol. Biomol. Spectrosc.* **2021**, *250*, 119316. [[CrossRef](#)]
51. Wang, S.; Xu, D.; Ma, L.; Qiu, J.; Wang, X.; Dong, Q.; Zhang, Q.; Pan, J.; Liu, Q. Ultrathin ZIF-67 nanosheets as a colorimetric biosensing platform for peroxidase-like catalysis. *Anal. Bioanal. Chem.* **2018**, *410*, 7145–7152. [[CrossRef](#)] [[PubMed](#)]
52. Bai, X.; Wang, S.; Yan, X.; Zhou, H.; Zhan, J.; Liu, S.; Sharma, V.K.; Jiang, G.; Zhu, H.; Yan, B. Regulation of cell uptake and cytotoxicity by nanoparticle core under the controlled shape, size, and surface chemistries. *ACS Nano* **2020**, *14*, 289–302. [[CrossRef](#)] [[PubMed](#)]
53. Wan, L.; Wu, L.; Su, S.; Zhu, D.; Chao, J.; Wang, L. High peroxidase-mimicking activity of gold@platinum bimetallic nanoparticle-supported molybdenum disulfide nanohybrids for the selective colorimetric analysis of cysteine. *Chem. Commun.* **2020**, *56*, 12351–12354. [[CrossRef](#)] [[PubMed](#)]

54. Sun, L.; Fu, Z.; Ma, E.; Guo, J.; Zhang, Z.; Li, W.; Li, L.; Liu, Z.; Guo, X. Ultrasmall Pt nanozymes immobilized on spherical polyelectrolyte brushes with robust peroxidase-like activity for highly sensitive detection of cysteine. *Langmuir* **2022**, *38*, 12915–12923. [[CrossRef](#)] [[PubMed](#)]
55. Jiang, C.; Wei, X.; Bao, S.; Tu, H.; Wang, W. Cu@Au(Ag)/Pt nanocomposite as peroxidase mimic and application of Cu@Au/Pt in colorimetric detection of glucose and l-cysteine. *RSC Adv.* **2019**, *9*, 41561–41568. [[CrossRef](#)] [[PubMed](#)]
56. Chen, C.; Wang, Y.; Zhang, D. Peroxidase-like activity of vanadium tetrasulfide submicrospheres and its application to the colorimetric detection of hydrogen peroxide and L-cysteine. *Microchim. Acta* **2019**, *186*, 784. [[CrossRef](#)] [[PubMed](#)]
57. Chen, Y.; Chen, T.; Wu, X.; Yang, G. CuMnO₂ nanoflakes as pH-switchable catalysts with multiple enzyme-like activities for cysteine detection. *Sensor. Actuat. B-Chem.* **2019**, *279*, 374–384. [[CrossRef](#)]
58. Lu, W.; Chen, J.; Kong, L.; Zhu, F.; Feng, Z.; Zhan, J. Oxygen vacancies modulation Mn₃O₄ nanozyme with enhanced oxidase-mimicking performance for L-cysteine detection. *Sensor. Actuat. B-Chem.* **2021**, *333*, 129560. [[CrossRef](#)]
59. Ravindran, A.; Mani, V.; Chandrasekaran, N.; Mukherjee, A. Selective colorimetric sensing of cysteine in aqueous solutions using silver nanoparticles in the presence of Cr³⁺. *Talanta* **2011**, *85*, 533–540. [[CrossRef](#)]
60. Chen, S.; Gao, H.; Shen, W.; Lu, C.; Yuan, Q. Colorimetric detection of cysteine using noncrosslinking aggregation of fluorosurfactant-capped silver nanoparticles. *Sensor. Actuat. B-Chem.* **2014**, *190*, 673–678. [[CrossRef](#)]
61. Neri, J.M.; Latochski, E.; de Araujo, J.G.L.; de Lima, R.P.; Cavalcanti, L.N.; Neves, A.C.O.; Gasparotto, L.H.S.; Domingos, J.B.; Menezes, F.G. Quinoxaline-functionalized silver nanoparticles as chromogenic probe for the multiple selective detection of cysteine, Mg²⁺ and Sn²⁺ in aqueous solution. *Sensor. Actuat. B-Chem.* **2021**, *349*, 130743. [[CrossRef](#)]
62. Liu, X.; Zhang, S.; Xu, H.; Wang, R.; Dong, L.; Gao, S.; Tang, B.; Fang, W.; Hou, F.; Zhong, L.; et al. Nitrogen-doped carbon quantum dots from poly(ethyleneimine) for optical dual-mode determination of Cu²⁺ and L-Cysteine and their logic gate operation. *ACS Appl. Mater.* **2020**, *12*, 47245–47255. [[CrossRef](#)]
63. Qu, X.; Zou, J.; Shen, Y.; Zhao, B.; Liang, J.; Wang, Z.; Zhang, Y.; Niu, L. High-efficiency peroxidase mimics for fluorescence detection of H₂O₂ and l-cysteine. *Analyst* **2022**, *147*, 1808–1814. [[CrossRef](#)]
64. Khamcharoen, W.; Henry, C.S.; Siangproh, W. A novel L-cysteine sensor using in-situ electropolymerization of L-cysteine: Potential to simple and selective detection. *Talanta* **2022**, *237*, 122983. [[CrossRef](#)]

Disclaimer/Publisher's Note: The statements, opinions and data contained in all publications are solely those of the individual author(s) and contributor(s) and not of MDPI and/or the editor(s). MDPI and/or the editor(s) disclaim responsibility for any injury to people or property resulting from any ideas, methods, instructions or products referred to in the content.